Direct numerical simulations of the Batchelor trailing vortex by a spectral method

M. Abid
Institut de Recherche sur les Phénomènes Hors Equilibre. UMR CNRS et Université d'Aix-Marseille I, service 252, Centre St-Jérôme, 13397 Marseille Cedex 20, France

M. E. Brachet
Laboratoire de Physique Statistique CNRS URA 1306, ENS Ulm 24 Rue Lhomond, 75231 Paris Cedex 05, France

(Received 16 January 1997; accepted 15 October 1997)

The nonlinear vorticity dynamics of the Batchelor trailing vortex is presented. Direct numerical simulations of the three-dimensional, incompressible, Navier-Stokes equations by a spectral method are used. It is shown that the initial vortex core is subjected to three transformations: a twisting phase, a lateral expansion of its cross section and formation of a spiral structure. These transformations are accompanied by a gradual deceleration of axial velocity. Mean kinetic energy is then transferred to radial velocity. When the transfer is maximum a secondary instability is initiated leading to the spiral structure. These transformations are in agreement with vortex breakdown observed in recent experiments. © *1998 American Institute of Physics.* [S1070-6631(98)00402-4]

I. INTRODUCTION

Using the boundary-layer-type approximation, Batchelor[1] derived a similarity solution of fluid equations for the flow in a trailing vortex far downstream. This solution depicts an axisymmetric swirling wake flow. The viscous and inviscid linear stability of this solution, in the limit of parallel flow, has been studied by Lessen, Singh and Paillet,[2] Leibovich and Stewartson,[3] Mayer and Powell,[4] Khorrami[5] and Duck and Khorrami.[6] In the inviscid case, no unstable axisymmetric disturbances were found. The perturbation with azimuthal wave number $m=1$ was found to have an unstable region of larger extent, in wave number, than any other. In the viscous case, the critical Reynolds numbers for the modes $m=0$ and $m=1$ are found to be 322,4 and 17,527 respectively.

In this paper, we use direct simulations of the three-dimensional incompressible Navier-Stokes equations (NSE) by a spectral method to account for the nonlinear vorticity dynamics of the Batchelor trailing vortex (BTV). We present the numerical method and its validation in sections II and III, respectively. The results are presented in section IV and sections V and VI are devoted to our discussion and conclusion, respectively.

II. NUMERICAL METHOD

We have chosen to use pseudo-spectral methods both for their precision and for their ease of implementation.[7] In order to exactly conserve energy in the constant density inviscid limit, and also to minimize storage, we use the so-called rotational formulation.[7] Specifically we solve

$$\frac{\partial \mathbf{u}}{\partial t} = -\nabla \Pi + \mathbf{u}\times\boldsymbol{\omega} + \nu \Delta \mathbf{u}, \quad \Pi = \frac{p}{\rho_0} + \frac{u^2}{2}, \quad \nabla\cdot\mathbf{u} = 0. \tag{1}$$

The Batchelor trailing vortex is the velocity field $\mathbf{u}=(0,W(r),U(r))$, where $U(r)$ and $W(r)$ are given by

$$U(r) = \exp(-(r/a)^2), \tag{2}$$

$$W(r) = q\frac{(1-\exp(-(r/a)^2))}{(r/a)}. \tag{3}$$

Here, r is the radial distance of a cylindrical coordinate system (r,ϕ,x) aligned with the vortex, q is the swirl intensity and a the vortex core size. The time is non-dimensionalized by $U(0)/a$ and the Reynolds number is fixed to $U(0)a/\nu = 1000$. In order to accommodate the profiles $U(r)$ and $W(r)$ of the vortex in a triply periodic Fourier representation, we consider a periodic array of vortices with transverse periodicity length $L_y = L_z = L$, greater than the vortex core $(L/a \sim 5)$, and a longitudinal periodicity length L_x in order to allow three-dimensional disturbances (see figure 1). To make $W(r)$ compatible with the periodic representation, we use

$$r_p = \frac{L}{2\pi}\sqrt{\sin^2\left(\frac{2\pi}{L}y\right) + \sin^2\left(\frac{2\pi}{L}z\right)}, \tag{4}$$

instead of

$$r = \sqrt{(y^2+z^2)}. \tag{5}$$

This periodic radial coordinate is easier than the so-called ''imbricate'' series.[8,9] It will be shown in section III that this definition does not affect the vortex dynamics.

As we are interested in the instabilities of an isolated vortex, and not the instabilities of an array of vortices, the planes $y=nL$, $z=mL$ can be taken as fixed free-slip boundaries. We thus expand the velocity field $\mathbf{u}=(u,v,w)$ as

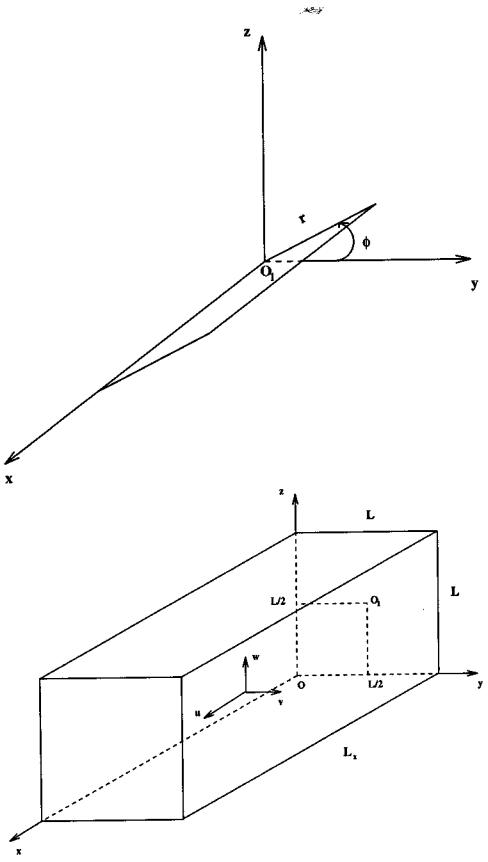

FIG. 1. Representation of the cylindrical coordinate system used in the definition of the Batchelor trailing Vortex (top) and of the integrating box (bottom). Note that the origin of the cylindrical coordinate system is O_1. The x, y and z velocity components are u, v and w respectively. The planes $y=nL$, $z=mL$ (n and m integers), are reflection symmetry planes of the flow. The axial periodicity length L_x allows three-dimensional disturbances.

$$u(x,y,z,t)=\sum_{k_x,k_y,k_z}\hat{u}(k_x,k_y,k_z,t)e^{ik_x x}\cos(k_y y)\cos(k_z z),$$

$$v(x,y,z,t)=\sum_{k_x,k_y,k_z}\hat{v}(k_x,k_y,k_z,t)e^{ik_x x}\sin(k_y y)\cos(k_z z), \tag{6}$$

$$w(x,y,z,t)=\sum_{k_x,k_y,k_z}\hat{w}(k_x,k_y,k_z,t)e^{ik_x x}\cos(k_y y)\sin(k_z z).$$

TABLE I. Fields lateral dependence.

Field	y dependence	z dependence
u	cosine	cosine
v	sine	cosine
w	cosine	sine
u^2	cosine	cosine
ω_x	sine	sine
ω_y	cosine	sine
ω_y	sine	cosine
$(\mathbf{u}\times\boldsymbol{\omega})_x$	cosine	cosine
$(\mathbf{u}\times\boldsymbol{\omega})_y$	sine	cosine
$(\mathbf{u}\times\boldsymbol{\omega})_z$	cosine	sine
p	cosine	cosine

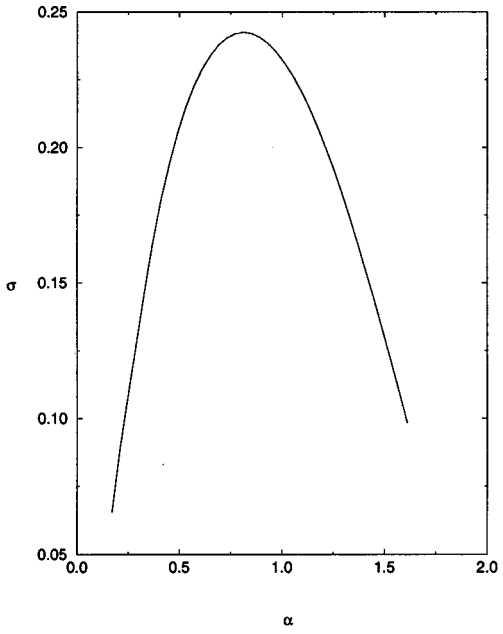

FIG. 2. Dispersion relation for $q=-0.458$ and $m=1$.

with

$$k_x=\frac{2\pi}{L_x}i_x, \qquad k_y=\frac{2\pi}{L_y}i_y, \quad k_z=\frac{2\pi}{L_z}i_z. \tag{7}$$

In the following, we will denote the resolution as $N_x\times N_y\times N_z$ when the limits of the sums (6) are $0\leqslant i_x<N_x, 0\leqslant i_y<N_y/2, 0\leqslant i_z<N_z/2$. By using these sine and cosine transformations in the lateral directions, we gain a

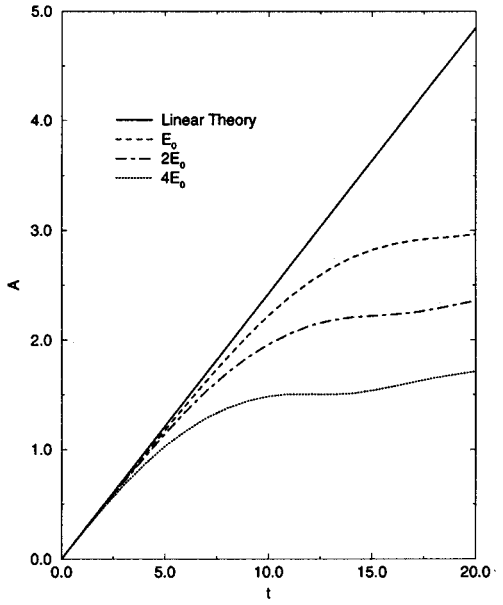

FIG. 3. Amplitude of the mode ($m=1$, $q=-0.458$) versus time for three different values of the energies of the perturbation E_0. Solid curve: linear theory. Discontinued curves: nonlinear calculations.

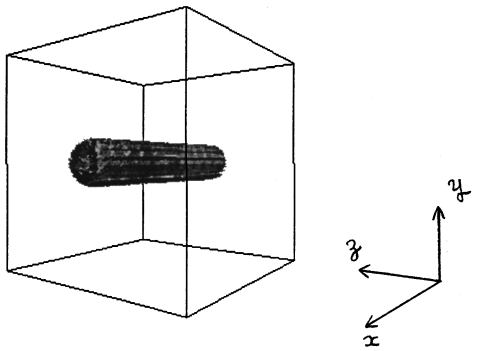

FIG. 4. A three-dimensional vector plot of the vorticity field of the BTV at $t=0$.

factor of 4 in storage and number of operations for the implementation in comparison with a general (complex) periodic transform. All fields are expanded in the same manner; Table I shows their lateral dependence.

By projecting on the space of divergence-free fields, (1) can be reduced to

$$\frac{\partial \hat{u}_m}{\partial t} = \sum_j \left(\delta_{mj} - \epsilon_{mj} \frac{k_m k_j}{k^2} \right) \widehat{(\mathbf{u} \times \boldsymbol{\omega})}_j - \nu k^2 \hat{u}_m , \tag{8}$$

where ϵ_{mj} is given by

$$[\epsilon_{mj}] = \begin{bmatrix} 1 & -i & -i \\ i & 1 & 1 \\ i & 1 & 1 \end{bmatrix}. \tag{9}$$

For temporal evolution, we have chosen to use an Adams-Bashforth Crank-Nicolson discretization scheme. Equations (8) are written in the following form:

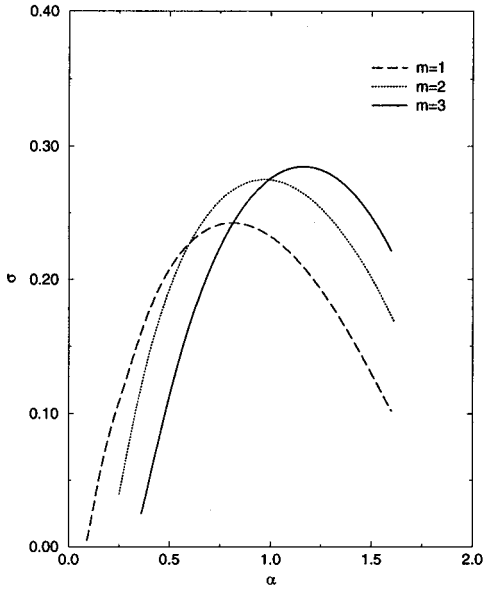

FIG. 5. Dispersion relations of the modes 1, 2 and 3 of BTV with $q=-0.458$.

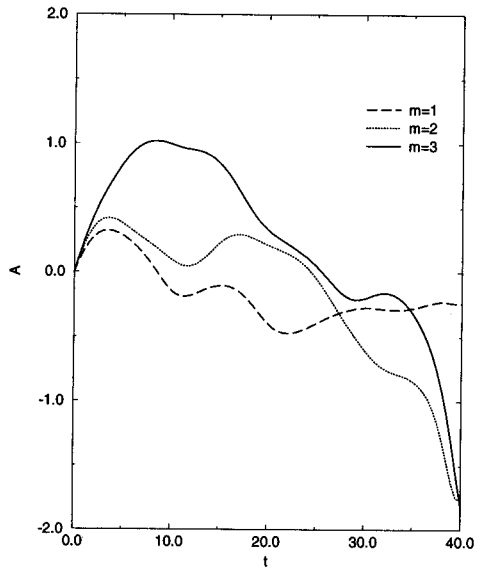

FIG. 6. Amplitudes of $m=1$, 2 and 3 modes versus time. Nonlinear calculations.

$$\frac{\partial \hat{u}_m}{\partial t} = \hat{C}_m - \hat{D}_m , \quad m=1,2,3, \tag{10}$$

where $\hat{C}_m$ is the nonlinear convective term and $\hat{D}_m$ the linear diffusive term in the Fourier space. Time integration scheme reads

$$\hat{u}_m^{n+1} = \frac{(1-\nu k^2 \Delta t/2)\hat{u}_m^n + (\Delta t/2)(3\hat{C}_m^n - \hat{C}_m^{n-1})}{(1+\nu k^2(\Delta t/2))}. \tag{11}$$

For the first time step, we use a backward Euler scheme

$$\hat{u}_m^1 = \hat{u}_m^0 + \Delta t[\hat{C}_m^0 - \hat{D}_m^0]. \tag{12}$$

This time stepping scheme is globally second-order accurate in time.

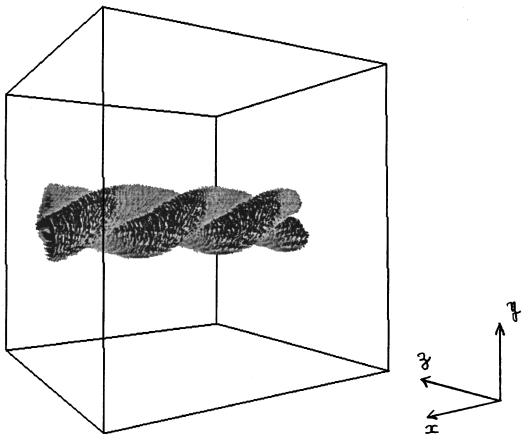

FIG. 7. A three-dimensional vector plot of the vorticity field at the time of saturation of the linear instability of the modes $m=1$ and $m=2$.

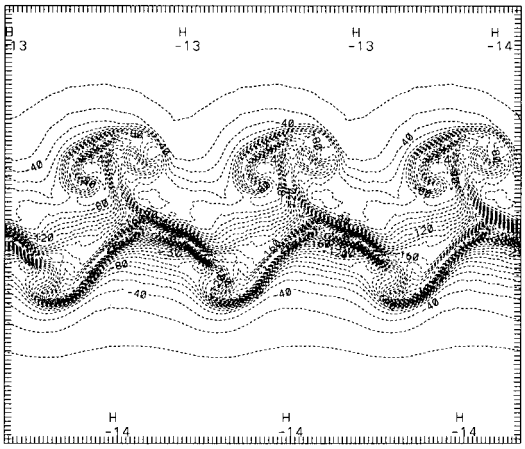

FIG. 8. Contour lines of a cross section ($x-y$ plane, $z=L/2$) of the pressure field just after the initiation of the secondary instability. Three integrating boxes are presented.

III. VALIDATION OF THE NUMERICAL METHOD

We use the linear stability results to validate the nonlinear temporal calculations. We solve, by a shooting method, the pressure equation of the linearized Euler equations for a Fourier mode $p(\mathbf{x},t)=\hat{p}(r)\exp(ikx+im\theta-i\omega t)$, $\omega=\omega_r+i\sigma$. The dispersion relation, $\sigma(k)$, with a swirl intensity $q=-0.458$ and $m=1$ is presented in figure 2. These values correspond to the most unstable helical mode.[4] Velocity eigenfunctions with the maximum growth rate $\sigma=0.2424$ are superposed to the basic velocity profile BTV as a small perturbation. The Navier-Stokes equations are then integrated and the growth rate of the perturbation calculated. Figure 3 shows that the nonlinear calculations reproduce the growth rate σ for small times. Three different energies of the perturbation are used. We see that in order to accelerate the manifestation of the nonlinear regime, we can multiply the initial energy of the perturbation by 4 without spoiling the quality of the growth rate. It is clear by looking at figures 2 and 3 that the transformation (4) does not affect the vortex dynamics.

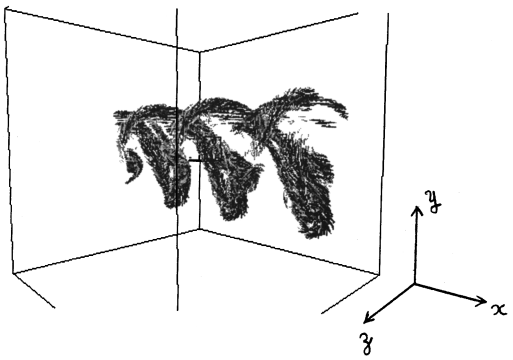

FIG. 9. Three-dimensional plot of the vorticity field at the same time as figure 8.

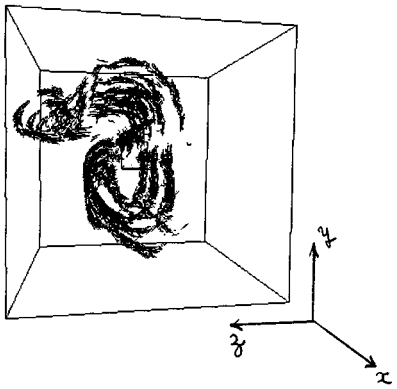

FIG. 10. Three-dimensional plot of the vorticity field at an advanced time.

IV. NUMERICAL RESULTS

The numerical results described herein are obtained with a resolution of $40\times200\times200$. We present in figure 4 a three-dimensional plot of the vorticity field of the BTV at initial time with $q=-0.458$. We use the three first linearly unstable modes as a perturbation to the BTV. Figure 5 shows the corresponding dispersion relations. We then follow their nonlinear evolution by integrating the incompressible Navier-Stokes equations. Figure 6 shows the different amplitudes versus time. We observe, for small times, a linear growth phase for the three modes. For $t=3$, we can see the nonlinear saturation of modes $m=1$ and $m=2$. To this state corresponds a formation of two helices of vorticity which twist together as shown in figure 7. After the saturation of the linear growth of the $m=3$ mode, an inhibition phase of the linear growth of the three modes occurs up to $t=12.5$. At this time, we can see a new growth of the modes $m=1$ and $m=2$ suggesting the initiation of a secondary instability. This secondary instability creates a lateral structure as shown in figure 8 which represents a cross section of the pressure field (we present three boxes of integration). To this structure

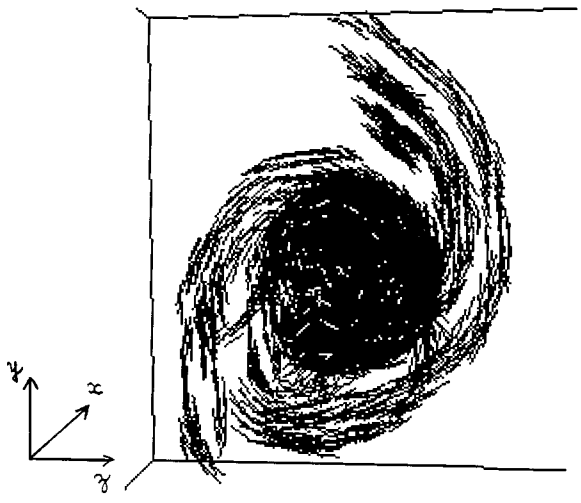

FIG. 11. Three-dimensional plot of the vorticity field at an advanced time when a random noise is used as a perturbation.

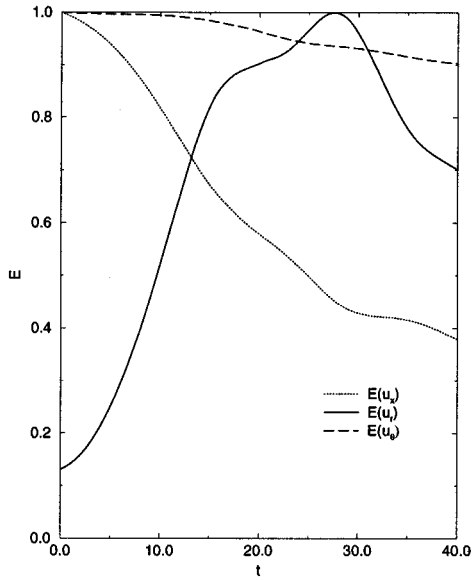

FIG. 12. Mean energies of the three velocity components: axial u_x, radial u_r and azimuthal u_θ versus time.

corresponds the formation of a lateral arm in the vorticity field as can be seen in figure 9: the initial structure has exploded. In figure 10, we present an advanced time of the exploded structure. We see the formation of many lateral arms that encircle the center of the structure, due to the rotation present in the flow, giving it a spiral form. We find the same breakdown mechanism of the BTV using random noise as initial perturbation rather than linearly unstable modes. We present in figure 11 the spiral form of the exploded structure that we obtain in this case.

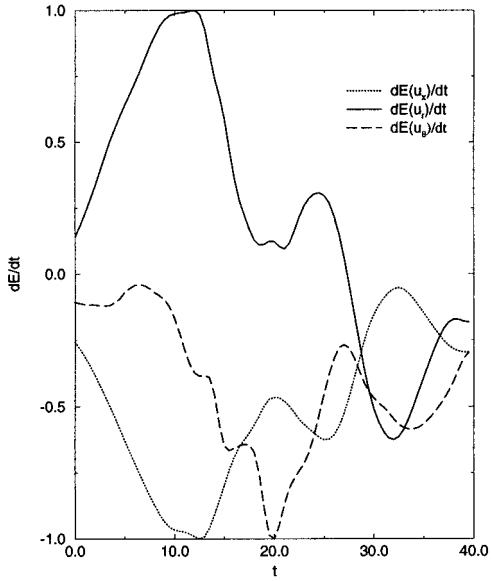

FIG. 13. Rates of energy transfer between the three velocity components: axial u_x, radial u_r and azimuthal u_θ versus time.

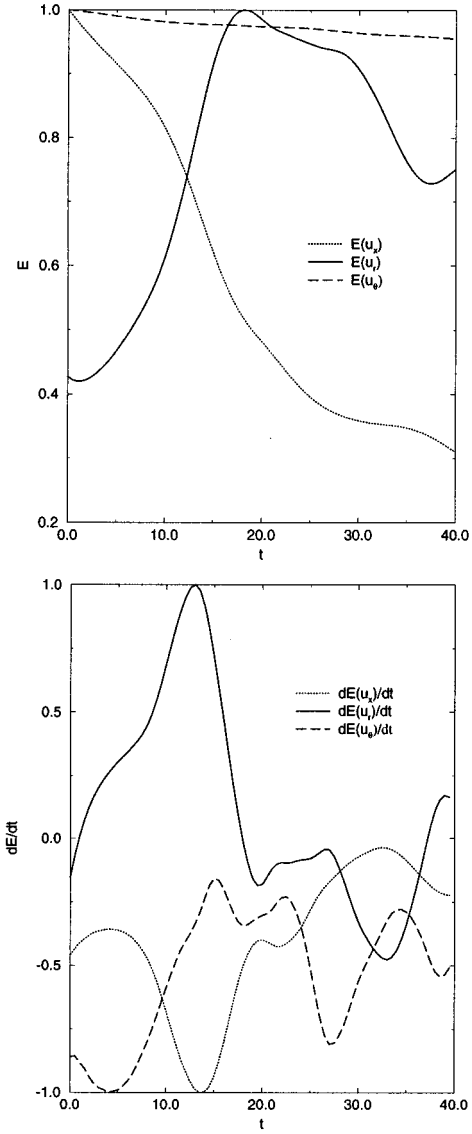

FIG. 14. Time dependence of mean energies (top) and rates of energy transfer (bottom) of the three velocity components in the same conditions as in figures 12 and 13 but with random noise as initial perturbation.

Let us define the spatial mean energy, $E(\Phi)$, of a scalar field, $\Phi(\mathbf{x},t)$ a function of the location $\mathbf{x}$ and time t, by

$$E(\Phi)=\frac{1}{\Omega}\int_{\Omega}\frac{\Phi^2}{2}(\mathbf{x},t)d\Omega, \tag{13}$$

where Ω stands for a volume of the fluid. By looking at the spatial mean energies of the three velocity field components: axial, radial and azimuthal we can explain the origin of the BTV breakdown and its lateral (radial) nature. Figure 12 shows the mean energies versus time. The azimuthal component (the swirl) is slightly affected by the evolution. In contrast, the mean energy of the axial component of the velocity is diminished. This corresponds to a deceleration of the flow. The deceleration is accompanied by an energy transfer to the radial velocity component. This can be understood by the

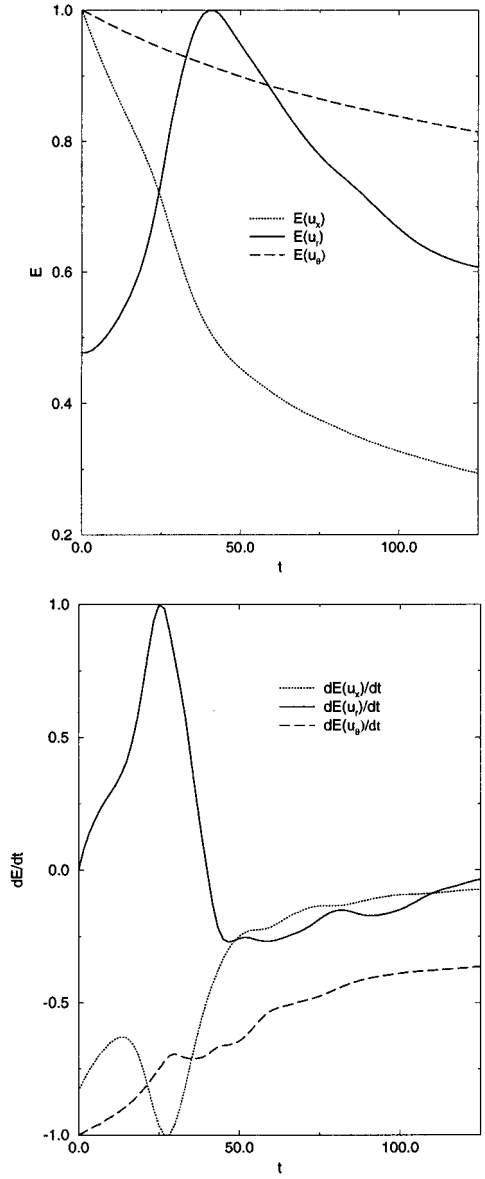

FIG. 15. Time dependence of mean energies (top) and rates of energy transfer (bottom) of the three velocity components in the same conditions as in figures 14 but with $q=0.8$. The change of sign of q corresponds to a change of the sign of the fluid rotation.

incompressibility of the flow. The transfer of energy is maximum at a time that coincides with the initiation of the secondary instability as shown in figure 13.

The same mechanism is found when we use a random noise as initial perturbation or another value of the swirl parameter q as seen in figures 14 and 15.

The mechanism of the BTV breakdown presented here is in accordance with that observed in recent experiments of turbulence.[10]

Finally, it is interesting to note that the BTV breakdown is also characterized by a simultaneous intensification of vorticity and dissipation. This is shown in figure 16 where $\omega^2_{max}=\max_{\mathbf{x}}|\boldsymbol{\omega}|^2$ and $\sigma^2_{max}=\max_{\mathbf{x}}\ 0.5\Sigma_{ij}(\partial_i u_j+\partial_j u_i)^2$ are plotted as functions of time. It is also interesting to note that

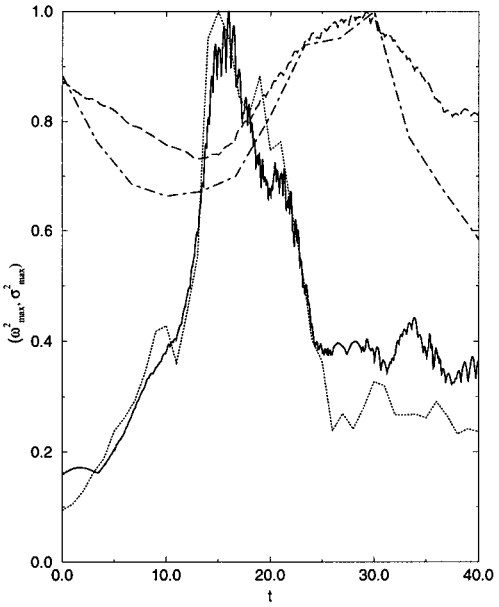

FIG. 16. Time dependence plots of $\omega^2{}_{max}$ (solid) and $\sigma^2{}_{max}$ (dot) for $q=-0.458$ and with linear modes as initial perturbations; $\omega^2{}_{max}$ (long-dash) and $\sigma^2{}_{max}$ (dot-dash) for $q=0.8$ and a random noise as initial perturbations.

the relative energy loss of the axial velocity between $t=0$ and the time of initiation of the secondary instability is always about 30% as shown in figure 17.

V. DISCUSSION

Vortex breakdown refers to ''an abrupt change in the structure of the core of swirling flow.'' [11] There are two pre-

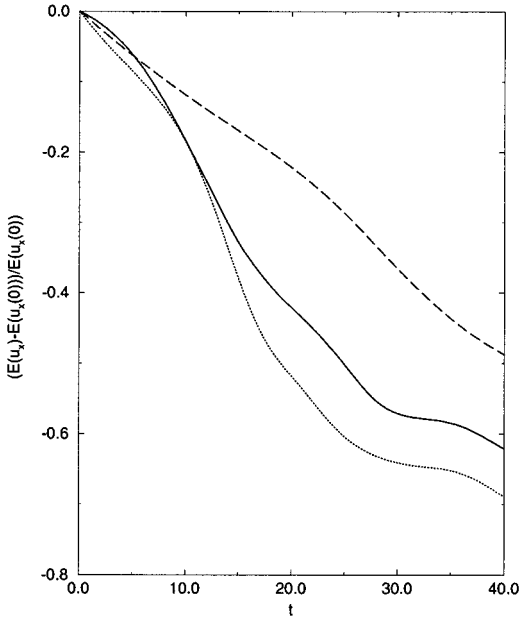

FIG. 17. Time dependence plots of relative energies of the axial velocity component u_x. Solid: $q=-0.458$ and with linear modes as initial perturbations. Dot: $q=-0.458$ and with random noise as initial perturbations. Dash: $q=0.8$ and with random noise as initial perturbations. The initial axial velocity is $u_x(0)$.

dominant forms of vortex breakdown: the nearly axisymmetric bubble and the nonaxisymmetric spiral type breakdown.[12] Ludewieg[13] and Jones[14] using linear instability theory concluded that the spiral-type is the basic mode of vortex breakdown. Experimental investigations of vortex breakdown were carried out in flows above delta wings at high angle of attack and in pipe flows. Bubble-type breakdown is characterized by a nearly axisymmetric region of reversed flow with a stagnation point at the forward end.[12] In the case of the spiral-type breakdown, when a dye filament is introduced on the vortex axis, ''the spiral form is marked by a kink in the filament followed by a corkscrew-shaped twisting of the dye.'' [15] ''The spiral form in particular reveals the suddenness of breakdown and suggests the occurrence of a stagnation point at the vortex axis.'' [16] The spiral structure rotates in the same sense as the surrounding fluid.[12]

Krause,[17] Krause and Althaus[18] stated that an adverse pressure gradient at large radial distances is extremely important in the initiation and development of vortex breakdown for an isolated slender vortex. The pressure gradient leads to a deceleration of the axial velocity component.[12] Conservation of mass requires radial out-flow. A redistribution of the axial into the circumferential vorticity component follows from the conservation of angular momentum and the vorticity transport equation.[12] The circumferential vorticity component induces an additional axial velocity component against the main flow direction. This leads to a stronger deceleration of the axial, and then enhancement of the radial, velocity components. Formation of a stagnation point on the axis of the slender vortex follows.[12] Brown and Lopez[19] also noted that deceleration on the axis of a slender vortex implies radial out-flow by conservation of mass. The straight and parallel vortex lines upstream of the point of deceleration are stretched and tilted in the region of radial out-flow. The vorticity vector acquires a circumferential component. The axial flow is then decelerated by induction, and stretching and tilting of the vortex lines are enhanced. ''This nonlinear interaction between stretching and tilting and deceleration of the axial flow may be promoted by a positive axial pressure gradient at larger radial distances.'' [12]

Many numerical simulations of vortex breakdown have been performed with an adverse pressure gradient applied at the lateral boundaries.[20–22] Good agreement with experiments was found. The numerical simulations herein are also in good agreement with experiments. But no adverse pressure gradient at lateral boundaries is imposed. Vortex breakdown still occurs. The temporal nature of calculations and the periodic boundary conditions prevent the formation of a stagnation point. Only the spiral-type breakdown is observed. The formation of a stagnation point in the flow is then not a necessary condition for the spiral-type breakdown to occur. The absence of an adverse pressure gradient also suggests that the initiation of deceleration of the axial velocity is a diffusive process in this case.

VI. CONCLUSION

We have accounted for the nonlinear vorticity dynamics of the Batchelor Trailing Vortex. We have shown that the flow undergoes deceleration accompanied by energy transfer from the axial velocity component to the radial one. When the energy transfer is maximum, a secondary instability is initiated. The vortex breaks down in the lateral direction; vorticity arms are formed, and the rotation of the flow rolls up these arms to give to the exploded BTV a spiral form. This mechanism is robust. It is reproduced for different initial conditions and different values of the swirl parameter q.

ACKNOWLEDGMENTS

The authors acknowledge fruitful discussions with Y. Couder, S. Douady, O. Cadot and L. Tuckerman. The computations were carried out on the 90/8 Cray computer of the Institut du Développement et des Ressources en Informatique Scientifique.

[1] G. K. Batchelor, ''Axial flow in the trailing line vortices,'' J. Fluid Mech. **20**, 645 (1964).
[2] M. Lessen, P. J. Singh, and F. Paillet, ''The stability of trailing line vortex. Part 1. Inviscid theory,'' J. Fluid Mech. **63**, 753 (1974).
[3] S. Leibovich and K. Stewrtson, ''A sufficient condition for the instablility of columnar vortices,'' J. Fluid Mech. **126**, 335 (1983).
[4] E. W. Mayer and K. G. Powell, ''Viscous and inviscid instabilities of a trailing vortex,'' J. Fluid Mech. **245**, 91 (1992).
[5] M. R. Khorrami, ''On the viscous modes of instability of a trailing-line vortex,'' J. Fluid Mech. **225**, 197 (1991).
[6] P. W. Duck and M. Khorrami, ''A note on the effects of viscosity on the stability of trailing-line vortex,'' J. Fluid Mech. **245**, 175 (1992).
[7] D. Gottlieb and S. A. Orszag, *Numerical Analysis of Spectral Methods* (SIAM, Philadelphia, 1977).
[8] A. Parker, ''Periodic solutions of the intermediate long-wave equation: A nonlinear superposition principle,'' J. Math. Phys. A **25**, 2005 (1992a).
[9] J. P. Boyd, *New Directions in Solitons and Nonlinear Periodic Waves: Polycnoidal Waves, Imbricated Solitons, Weekly Non-local Solitary Waves and Numerical Boundary Value Algorithms*, Vol. 27. edited by T. Y. Wu and J. W. Hutchinson (Academic, New York, 1989b), pp. 1–82.
[10] O. Cadot, S. Douady, and Y. Couder, ''Characterization of the low-pressure filaments in a three-dimensional turbulent shear flow,'' Phys. Fluids **7**, 630 (1995).
[11] T. B. Benjamin, ''Theory of the vortex breakdown phenomenon,'' J. Fluid Mech. **14**, 593 (1962).
[12] M. Wiemer W. Althaus, CH. Bruker, *Fluid Vortices* (Kluwer Academic, Dordtrecht, 1995).
[13] H. Ludewieg, ''Explanation of vortex breakdown by the stability theory for spiralling flows,'' IUTAM Symposium on Vortex Motions, Ann. Arbor, 1964.
[14] J. P. Jones, ''On the explanation of vortex breakdown,'' IUTAM Symposium on Vortex Motions, Ann. Arbor, 1964.
[15] S. Leibovich, ''The structure of vortex breakdown,'' Annu. Rev. Fluid Mech. **10**, 221 (1978).
[16] M. P. Escudier, ''Vortex breakdown: Observations and explanations,'' Prog. Aerosp. Sci. **25**, 189 (1988).
[17] E. Krause, ''The solution to the problem of vortex breakdown,'' Lect. Notes Phys. **371**, 35 (1990).
[18] E. Krause and W. Althaus, ''Vortex breakdown: Mechanism of initiation and change of mode,'' *Workshop on Analysis and Testing of High Angle of Attack Aerodynamics*, 1992, Tokyo, Japan.
[19] G. L. Brown and J. M. Lopez, ''Axisymmetric vortex breakdown. Part 2: Physical mechanism,'' J. Fluid Mech. **221**, 553 (1990).
[20] R. E. Spall and T. B. Gatski, ''A computational study of the taxonomy of vortex breakdown,'' AIAA J. **1990**, 1624 ().
[21] T. B. Gatski and R. E. Spall, ''Numerical study of vortex breakdown: From helices to bubbles,'' Fourth Int. Symposium on Comp. Fluid Dynamics, **I**, 418 (1991).
[22] M. Bruer and D. Hanel, ''A dual time-stepping method for 3-d, viscous, incompressible vortex flows,'' Comput. Fluids **22**, 467 (1993).